

Effects of a Non-Maxwellian EEDF on the scattering spectra of SRS and SBS

Jie Qiu^a, Ning Yang^a, Liang Hao^a

^a*Institute of Applied Physics and Computational Mathematics, Beijing, 100094, China*

Contents

1	Introduction	2
2	Theoretical analysis	3
3	Results and Discussion	4
4	Conclusion	12

arXiv:2011.07463v1 [physics.plasm-ph] 15 Nov 2020

Email: hao_liang@iapcm.ac.cn (Liang Hao)

ABSTRACT

In a laser-irradiated plasma, Langdon heating effect would result in a super-Gaussian EEDF. In this work, using the linear analysis, we have obtained the influence of a super-Gaussian EEDF on the best-matching wavelength of the scattered wave and linear gain of SRS and SBS for various plasma conditions. The influence of a super-Gaussian EEDF on the SRS and SBS is found to be distinct: for SRS, there is a redshift or blueshift of the scattered wave depending on the plasma condition; while for SBS, a super-Gaussian EEDF results in a redshift of the scattered wave compared to a Maxwellian EEDF. Furthermore, a super-Gaussian EEDF always enhances the SRS gain, while its effect on the SBS gain depends on the ion species, ion charge and ion ratio in a complex way.

Keywords Langdon, EEDF, SRS, SBS, gain, spectra

1 Introduction

Stimulated backward Raman scattering (SRS) and simulated backward Brillouin scattering (SBS), are three-wave interaction process where an incident electromagnetic wave (EMW) decays into a backscattered EMW and a forward propagating electron plasma wave (EPW) or ion acoustic wave (IAW). They are detrimental to inertial confinement fusion (ICF), since the backscattered light can take energy away from the incident laser, and the hot electrons generated by SRS can preheat the capsule [1].

Experimentally, the spectra of the backscattered light is one important diagnostic for the SRS and SBS process. Currently, the investigation of the scattered spectra usually assumes a Maxwellian electron energy distribution function (EEDF) [2, 3]. However, for plasmas in ICF, the dominant heating mechanism is inverse bremsstrahlung heating. And it is known that when the heating rate of inverse bremsstrahlung exceeds the electron thermal rate, the EEDF would deviate from the Maxwellian EEDF and become super-Gaussian [4, 5]. Known as the Langdon effect, it is especially significant for strong laser intensity or high-Z plasmas. Consequently, at least in some plasma region, such as the high-Z hohlraum-wall plasma in an indirect-driven ICF, or the multibeam overlapping region, the Langdon effect should be important. Recently, Langdon effect was observed in experiments and found to be important to crossed beam energy transfer (CBET) when multibeam irradiate at the plasma target, which could be a possible reason for the discrepancy between simulated gain of CBET and experimental results on NIF facility [6, 7]. On the other hand, there is also some discrepancy between the experimentally measured SRS spectra and the simulated result by the ray-tracing method [8]. One possible source of the discrepancy is the assumption of a Maxwellian EEDF in the current physics model of the ray-tracing method. To aid in addressing these issues, we have analyzed the influence of a super-Gaussian EEDF on the best-matching wavelength and linear gain of SRS and SBS for various plasma conditions in this work.

This paper is organized as follows: In Section 2, the theoretical analysis method is specified. In Section 3, the influence of a super-Gaussian EEDF on the best-matching wavelength and linear gain is discussed for SRS and SBS processes under various plasma conditions. In Section 4, the main conclusions are given.

2 Theoretical analysis

We use the super-Gaussian function to describe a non-Maxwellian electron energy distribution function (EEDF) distorted by the Langdon heating [4, 5],

$$f_{e0}(v) = \frac{n_e m}{4\pi v_{\text{th},e}^3 \beta_m^3 \Gamma(3/m)} \exp\left[-\left(\frac{v}{\beta_m v_{\text{th},e}}\right)^m\right] \quad (1)$$

where $v_{\text{th},e} = \sqrt{T_e/m_e}$, Γ is the gamma function, $5 \geq m \geq 2$ is the super-Gaussian exponent, and the factor $\beta_m = \sqrt{\frac{3\Gamma(3/m)}{\Gamma(5/m)}}$. A higher value of m indicates a more significant Langdon heating effect. At $m = 2$, the EEDF degenerates to a Maxwellian EEDF.

The kinetic electron susceptibility is given by [9]

$$\chi_e = \frac{\omega_{pe}^2}{k^2} \int \frac{\mathbf{k} \cdot \partial f_{e0} / \partial \mathbf{v}}{\omega - \mathbf{k} \cdot \mathbf{v}} d\mathbf{v} = \frac{\omega_{pe}^2}{k^2} \int_{-\infty}^{\infty} \frac{\partial f_{e0}^x / \partial v_x}{\omega/k - v_x} dv_x \quad (2)$$

where ω_{pe} is the electron plasma frequency, and the 1D distribution function $f_{e0}^x(v_x) = \iint f_{e0}(v_x, v_y, v_z) dv_y dv_z$. Since f_{e0} is isotropic, we have

$$f_{e0}^x(v_x) = 2\pi \int_{|v_x|}^{\infty} f_{e0}(v) v dv, \quad (3)$$

then χ_e can be written as

$$\chi_e = \frac{\omega_{pe}^2}{k^2} \frac{1}{\int_{-\infty}^{\infty} f_{e0}(v_x) v_x^2 dv_x} \int_{-\infty}^{\infty} \frac{f_{e0}(v_x) v_x}{v_x - \omega/k} dv_x \quad (4)$$

Taking $v_x = \beta_m v_{\text{th},e} u$, χ_e can be further transformed into

$$\chi_e(\omega, k) = \frac{1}{\beta_m^2 k^2 \lambda_{De}^2} \left[\int_{-\infty}^{\infty} f_{e0}(u) u^2 du + \frac{\omega}{\beta_m v_{\text{th},e} k} \int_{-\infty}^{\infty} \frac{f_{e0}(u)}{u - \frac{\omega}{\beta_m v_{\text{th},e} k}} du \right] \quad (5)$$

The dispersion relation of EPW is given by $\chi_e(\omega_l + j\nu_l, k_l) + 1 = 0$, where k_l , ω_l and ν_l are the wave number, frequency and Landau damping of EPW, respectively.

The stimulated Raman scattering (SRS) and stimulated Brillouin scattering (SBS), as resonant three-wave instabilities, require frequency and wave-number matching conditions [10]:

$$\omega_0 = \omega_s + \omega_{l,a} \quad (6)$$

$$k_0 = k_s + k_{l,a} \quad (7)$$

where ω_i and k_i are the frequencies and wavenumbers of incident laser ($i = 0$), scattering light ($i = s$) and electron plasma wave ($i = l$) or ion acoustic wave ($i = a$).

The probability for SRS or SBS can be measured by their linear gains,

$$G_{R,B} = \int_0^L \kappa_{R,B}(z) dz, \quad (8)$$

where the subscript R or B denotes the SRS or SBS process, L is the plasma length, and the spatial growth rate $\kappa_{R,B}$ obtained by the kinetic theory is given by [11, 1],

$$\kappa_{R,B}(\omega_s) = \frac{1}{4} \frac{k_{l,a}^2 v_{os}^2}{k_s c^2} \text{Im} \left[\frac{\chi_e(1 + \sum_{\alpha} \chi_{i\alpha})}{\epsilon(\omega_0 - \omega_s, k_0 - k_s)} \right] \quad (9)$$

where $v_{os} \equiv eE_0/m\omega_0$ is the electron quiver velocity with E_0 as the amplitude of the incident laser, $\chi_{i\alpha}$ is the susceptibility of ion species α , $\epsilon = 1 + \chi_e + \sum_{\alpha} \chi_{i\alpha}$ is the dielectric function for the EPW or IAW at frequency $\omega_{l,a} = \omega_0 - \omega_s$ and wave number $k_{l,a} = k_0 - k_s$. The incident laser and scattering light satisfies the dispersion relation for EMW,

$$\omega_{0,s}^2 = \omega_{pe}^2 + c^2 k_{0,s}^2. \quad (10)$$

For ions, a Maxwellian distribution with the same temperature T_i for all the species is assumed, yielding the ion susceptibility [9],

$$\chi_{i\alpha}(\omega, k) = \frac{1}{k^2 \lambda_{D\alpha}^2} [1 + \zeta Z(\zeta)], \quad (11)$$

where $Z(\zeta)$ is the plasma dispersion function with $\zeta \equiv \omega/\sqrt{2}v_{th,\alpha}k$, the thermal speed $v_{th,\alpha} = \sqrt{T_i/m_\alpha}$, the Debye length $\lambda_{D\alpha} = v_{th,\alpha}/\omega_{p\alpha}$ with $\omega_{p\alpha} = \sqrt{e^2 Z_\alpha^2 n_{i\alpha}/\epsilon_0 m_\alpha}$ being the plasma frequency of species α .

The gain peaks at the resonant frequencies at which the dielectric function $\epsilon = 1 + \chi_e + \sum_{\alpha} \chi_{i\alpha} \approx 0$. From (9), near the gain peak, we have

$$G_{R,B}(\omega_s) \propto \frac{-\mathcal{D}^I}{(\mathcal{D}^R)^2 + (\mathcal{D}^I)^2} \quad (12)$$

where

$$\mathcal{D} \equiv \frac{1}{\chi_e} + \frac{1}{1 + \sum_{\alpha} \chi_{i\alpha}}, \quad (13)$$

\mathcal{D}^I and \mathcal{D}^R are the imaginary and real parts of \mathcal{D} , respectively. At the resonant frequency ω_{s0} where $\mathcal{D}^R \approx 0$, we have

$$G_{R,B}(\omega_{s0}) \propto \frac{-1}{\mathcal{D}^I} \propto \nu_{l,a}^{-1} \quad (14)$$

where $\nu_{l,a}$ is the Landau damping of EPW or IAW. From (12), also it can be seen that the width $\Delta\omega_s$ of the gain versus frequency is determined by

$$|\mathcal{D}^R(\omega_{s0} \pm \Delta\omega_s)| \approx |\mathcal{D}^I|. \quad (15)$$

3 Results and Discussion

In this section, we investigate the influence of a super-Gaussian EEDF on the SRS and SBS using the linear gain given in (8). A uniform plasma is assumed, for which a wide range of electron temperature and electron density, i.e., $T_e \sim 0.1-8$ KeV and $n_e \sim 0.01-0.25 n_c$, is investigated. Here n_c is the critical density for the incident laser; the wavelength of incident light is assumed to be $\lambda_0 = 0.351 \mu\text{m}$. For the SBS process, different ion species and ion ratios, including low-Z plasmas with single ion species (H or He), low-Z plasmas with multiple ion species (H/He or CH), intermediate-Z plasmas with multiple ion species (CO_2), high-Z plasmas typical of ablation from hohlraum wall (Au, AuB, or UN), are investigated. These plasma conditions are common in ICF [1].

As shown in Figure 1, for the SRS process, the influence of a super-Gaussian EEDF on the best matching wavelength of the backscattered light where the gain peaks, depends on the electron density n_e and electron temperature T_e . Roughly speaking, at high n_e and low T_e ,

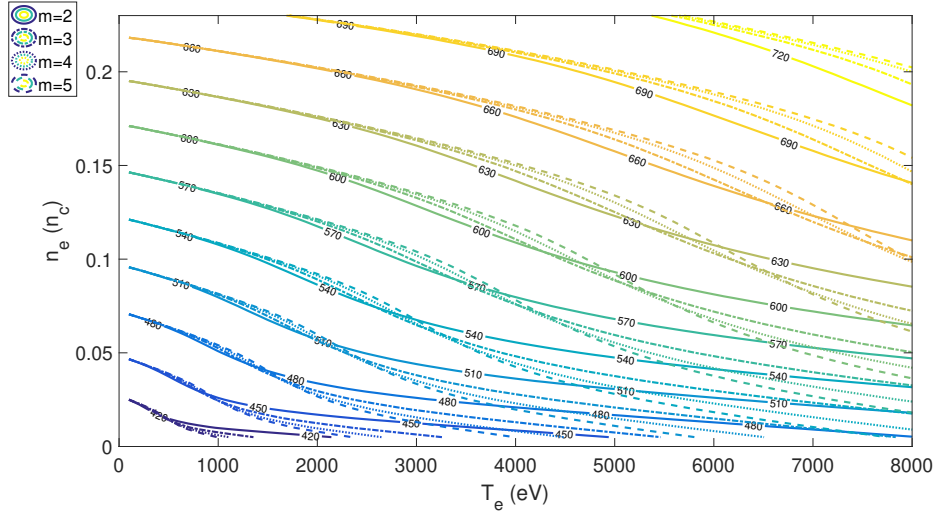


Figure 1: Raman scattered wavelength versus n_e and T_e for super-Gaussian EEDFs with different exponents m . The pump wavelength $\lambda_0 = 0.351 \mu\text{m}$ is assumed.

the best matching wavelength decreases with the super-Gaussian exponent m ; whereas at low n_e and high T_e , the best matching wavelength increases with m . For the former, we show the curve of the spatial growth rate (κ_R) versus scattered wavelength (λ_R) at the parameters (case I) $n_e = 0.1 n_c$, $T_e = 3 \text{ KeV}$ and the pump intensity $I_0 = 10^{15} \text{ W/cm}^2$ in Figure 2; while for the latter, the curve κ_R versus λ_R is shown in Figure 3 for the parameters (case II) $n_e = 0.05 n_c$, $T_e = 5 \text{ KeV}$ and $I_0 = 10^{15} \text{ W/cm}^2$. Clearly we can see the different behaviours of the wavelength shift with m at each condition. To understand this, the dispersion relation of EPW at different m is shown in Figure 4. By normalizing the frequency to ω_{pe} and the wavenumber to $1/\lambda_{De}$, a unified dispersion relation not dependent on other parameters such as n_e and T_e , is obtained. To show the matching point of SRS, the (normalized) dispersion relation of the scattered wave $(\omega_0 - \omega_l)^2 = \omega_{pe}^2 + c^2(k_0 - k_l)^2$ is also plotted. It can be seen that for case I, $k_l \lambda_{De} \sim 0.36$, the EPW frequency decreases with m , resulting in the increase of frequency (and hence the decrease of wavelength) of the scattered wave with m . While for case II, $k_l \lambda_{De} \sim 0.68$, the EPW frequency increases with m , resulting in the decrease of frequency (and hence the increase of wavelength) of the scattered wave with m .

From Figures 2 and 3, also we can see that for both cases the peak growth rate κ_R increases with m , and the width of the curve κ_R versus λ_R decreases with m . The anti-correlation of the peak growth rate and the width can be understood from (14) and (15): for SRS, $\mathcal{D} = 1/\chi_e + 1$, near the resonance, $\chi_e + 1 \approx 0$, that is, $\chi_e^R \approx -1$ and $\chi_e^I \approx 0$, hence $\mathcal{D}^I = -\chi_e^I/|\chi_e|^2 \approx -\chi_e^I$, and $\mathcal{D}^R = 1 + \chi_e^R/|\chi_e|^2 \approx 1 + \chi_e^R$. So from (14), $G_R \propto 1/\chi_e^I \propto 1/\nu_l$; while from (15), the width is determined by $|1 + \chi_e^R| \approx \chi_e^I \propto \nu_l$. Clearly, a smaller damping ν_l will result in a higher gain yet smaller width of the gain curve. From Figure 5, the Landau damping ν_l decreases with m , leading to the increase of gain and decrease of width of the gain curve with m .

The variation of Brillouin scattered wavelength with n_e and T_e at different super-Gaussian exponents for the typical cases of low-Z and high-Z plasmas are shown in Figure 6 and Figure 7, respectively. It can be seen that although the dependence of the best matching wavelength on n_e and T_e manifests distinct characteristics for low-Z and high-Z plasmas, the best matching wavelength of the backscattered light always increases with m , regardless of n_e and T_e . This can be understood from χ_e given in (16) in the limit of $\omega/k \ll v_{th,e}$. Ignoring the second term

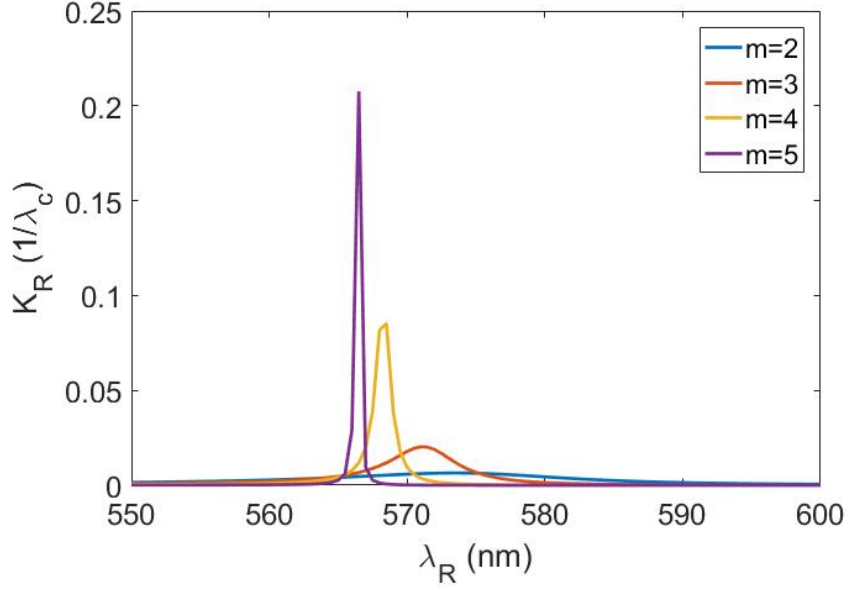


Figure 2: The spatial growth rate (κ_R) versus scattered wavelength (λ_R) at different super-Gaussian exponents m . The condition $n_e = 0.1 n_c$, $T_e = 3$ KeV and $I_0 = 10^{15}$ W/cm² (case I) is taken.

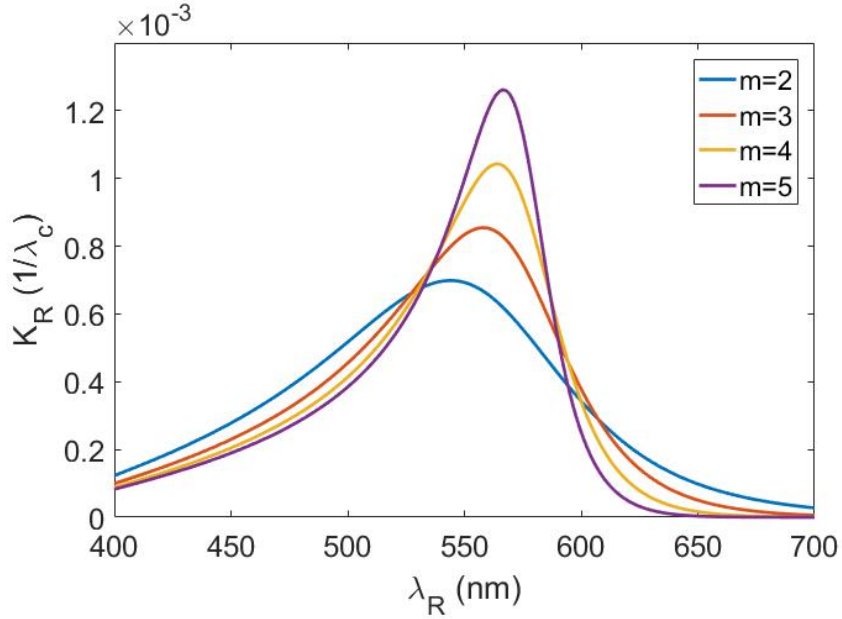


Figure 3: The spatial growth rate (κ_R) versus scattered wavelength (λ_R) at different super-Gaussian exponents m . The condition $n_e = 0.05 n_c$, $T_e = 5$ KeV and $I_0 = 10^{15}$ W/cm² (case II) is taken.

in this equation, we have

$$\chi_e^m(\omega, k) \approx \frac{\int_{-\infty}^{\infty} \exp[-u^m] du}{\beta_m^2 k^2 \lambda_{De}^2 \int_{-\infty}^{\infty} \exp[-u^m] u^2 du} = \frac{1}{A_m k^2 \lambda_{De}^2} \quad (16)$$

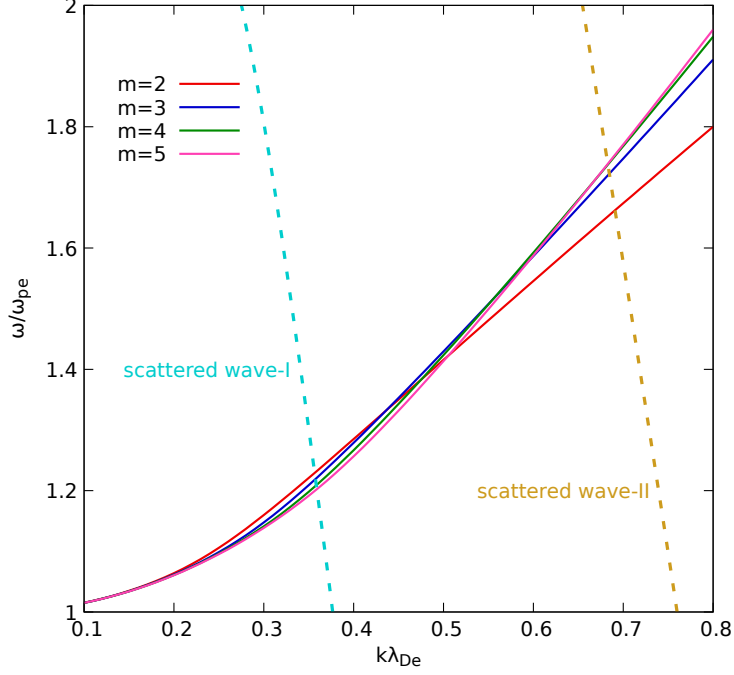


Figure 4: The dispersion relations of EPW (solid lines) at different super-Gaussian exponents. The dashed lines show the dispersion relation of the scattered wave $(\omega_0 - \omega_l)^2 = \omega_{pe}^2 + c^2(k_0 - k_l)^2$ for case I and case II. The intersection points of the curves for the EPW and for the scattered wave give the resonance wave number and frequency.

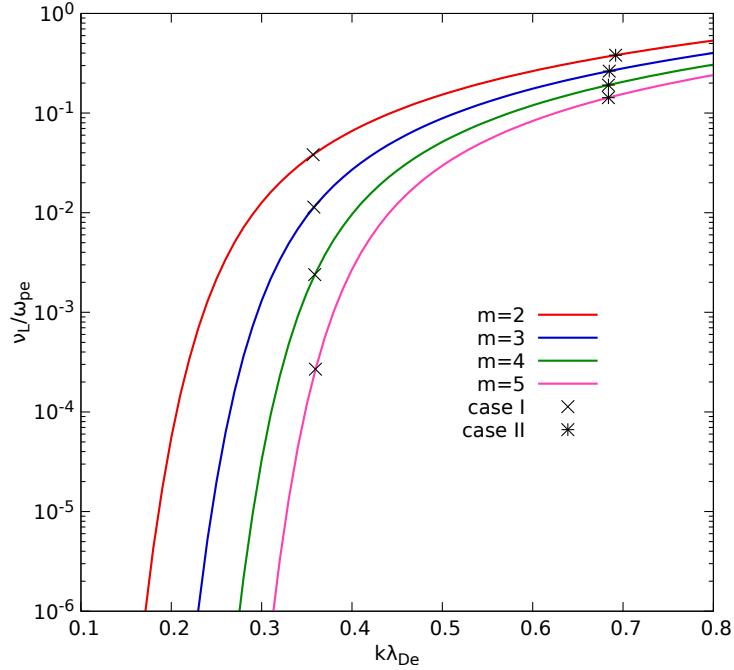


Figure 5: The Landau damping of EPW at different super-Gaussian exponents m . The matching points of Case I and Case II are indicated on the damping curves for each m .

where $A_m = 3\Gamma^2(3/m)/[\Gamma(1/m)\Gamma(5/m)]$, and the values of A_m at $m = 2, 3, 4, 5$ are 1, 1.24, 1.37 and 1.45, respectively. The increase of A_m with m implies a reduced number of slow electrons to shield the ions [12]. We can think that the Debye shielding electron temperature is

effectively boosted to $T_e A_m$. Since the ion acoustic velocity c_s is proportional to $\sqrt{T_e}$ (when ignoring the small contributions of ion thermal motion), it can be expected the IAW frequency $\omega_a = k_a c_s$ increases with m . Consequently, the frequency (wavelength) of the scattered wave decreases (increases) with m .

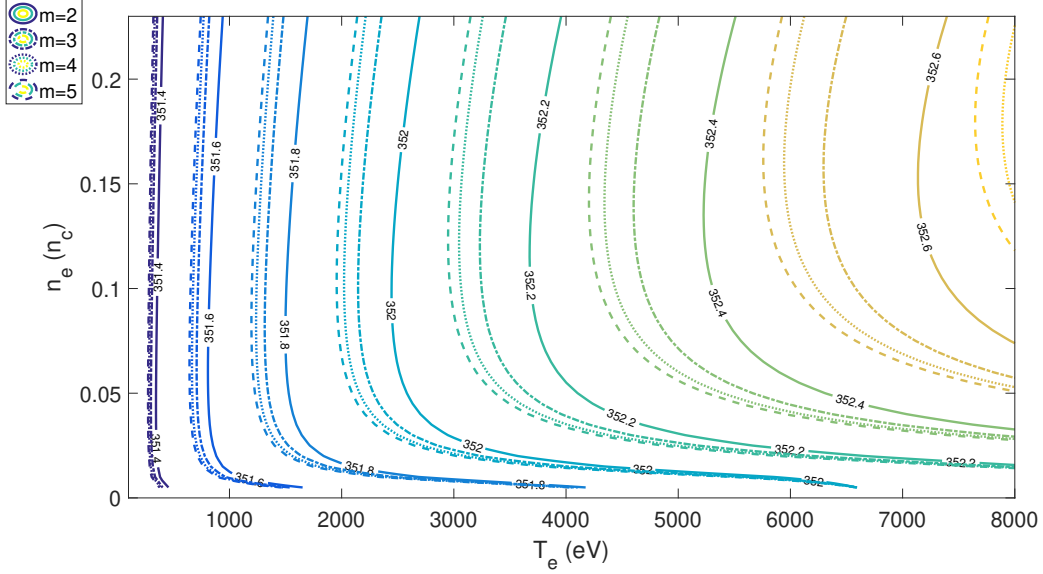


Figure 6: Brillouin scattered wavelength versus n_e and T_e for super-Gaussian EEDFs with different exponent m . Here a fully ionized He plasma with $T_e/T_i = 5$ is assumed; the pump wavelength $\lambda_0 = 0.351 \mu\text{m}$.

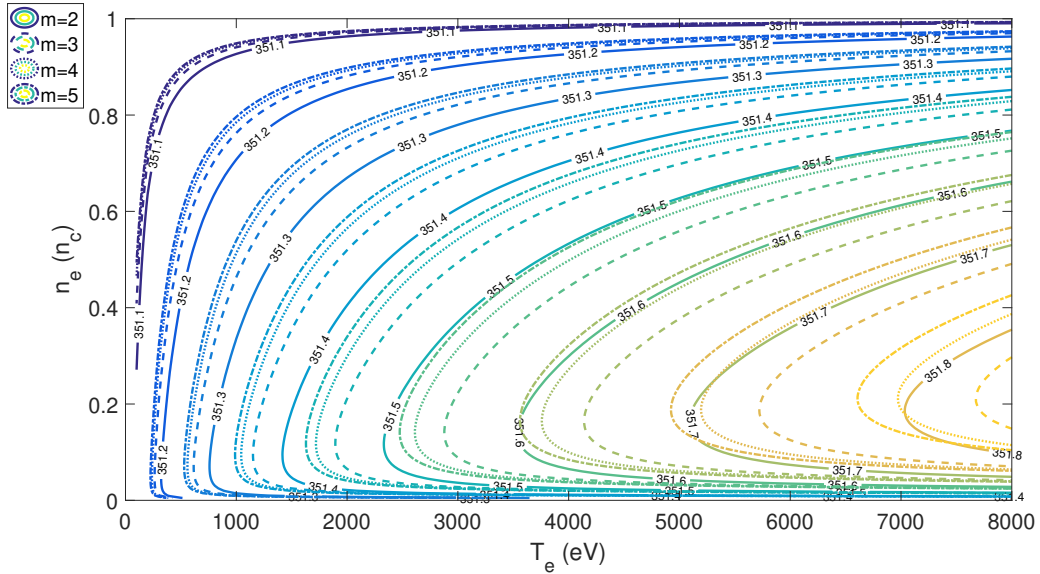


Figure 7: Brillouin scattered wavelength versus n_e and T_e for super-Gaussian EEDFs with different exponent m . Here a Au plasma with $T_e/T_i = 2$ and $Z = 50$ is assumed; the pump wavelength $\lambda_0 = 0.351 \mu\text{m}$.

However, the influence of the super-Gaussian exponent m on the peak gain of SBS is quite complex:

1. For plasmas with low-Z single species (e.g., H or He), the peak gain (or spatial growth rate κ_B) increases with m , as shown in Figure 8 for He plasma.
2. For plasmas with low-Z multiple species (e.g., H/He or CH), κ_B decreases with m , as shown in Figure 9 for H/He plasma.
3. For plasmas with intermediate-Z multiple species (e.g., CO₂), κ_B decreases with m , as shown in Figure 10 for CO₂ plasma.
4. For plasmas with high-Z single species (e.g., Au or U), κ_B decreases with m , as shown in Figure 11 for Au plasma.
5. For plasmas with high-Z/intermediate-Z multiple species (e.g., AuB or UN), in AuB plasma, κ_B decreases with m , as shown in Figure 12; whereas in UN plasma, as shown in Figure 13, κ_B versus m is no longer monotonic: κ_B firstly increases with m , then decreases with m with the maximum appearing between $m = 3$ and $m = 4$.

It can be seen the trend of the peak gain with m depends on the ion species and ion species ratios. Especially, the trend in multiple species plasma is generally different from that in single species plasma.

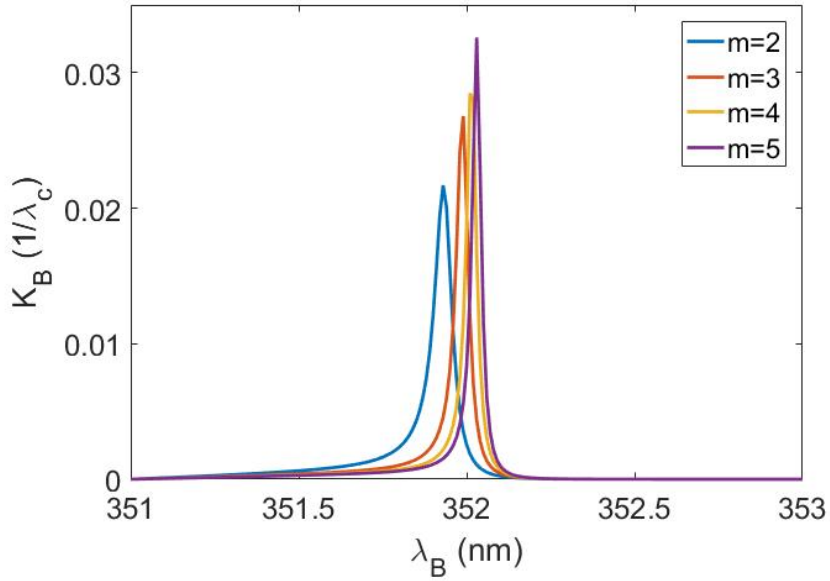


Figure 8: The convective spatial growth rate (κ_B) of SBS versus scattered wavelength (λ_B) at different super-Gaussian exponents m in fully ionized He plasma. The condition $n_e = 0.1 n_c$, $T_e = 3$ KeV, $T_i = T_e/5$ and $I_0 = 10^{15}$ W/cm² is taken.

To understand the influence of the super-Gaussian exponent on the gain of SBS, still we start from equation (14). Notice for the IAW, the Landau damping of IAW is contributed by both electrons and ions,

$$-\mathcal{D}^I = -\text{Im}\left[\frac{1}{\chi_e}\right] - \text{Im}\left[\frac{1}{1 + \sum_{\alpha} \chi_{i\alpha}}\right]. \quad (17)$$

Next we use the first term and the second term in the above equation to represent the damping due to electrons and ions, respectively. The phase velocity $v_{\text{ph}} \equiv \omega_{\alpha}/k_{\alpha}$ of IAW increases with

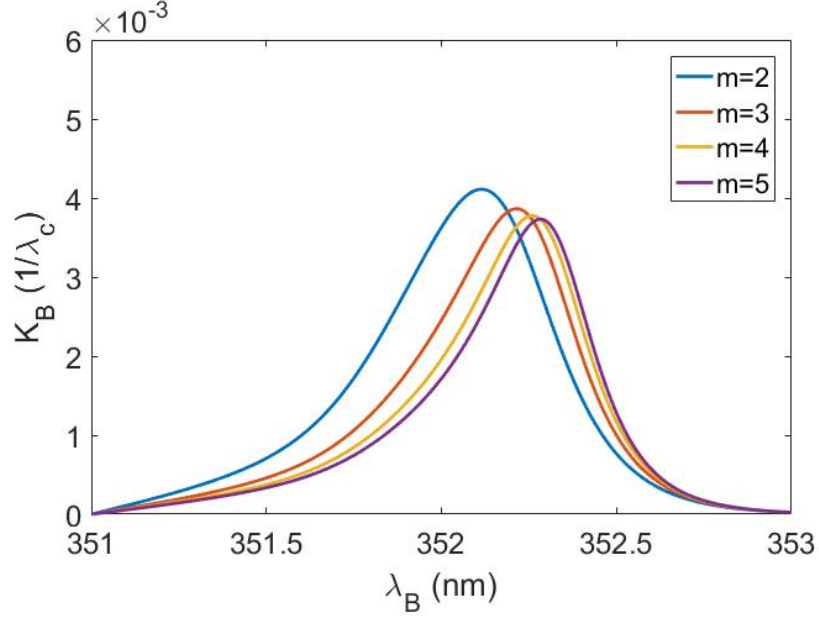


Figure 9: The convective spatial growth rate (κ_B) of SBS versus scattered wavelength (λ_B) at different super-Gaussian exponents m in fully ionized H/He plasma. The condition $n_e = 0.1 n_c$, $T_e = 3$ KeV, H/He=1:1, $T_i = T_e/5$ and $I_0 = 10^{15}$ W/cm² is taken.

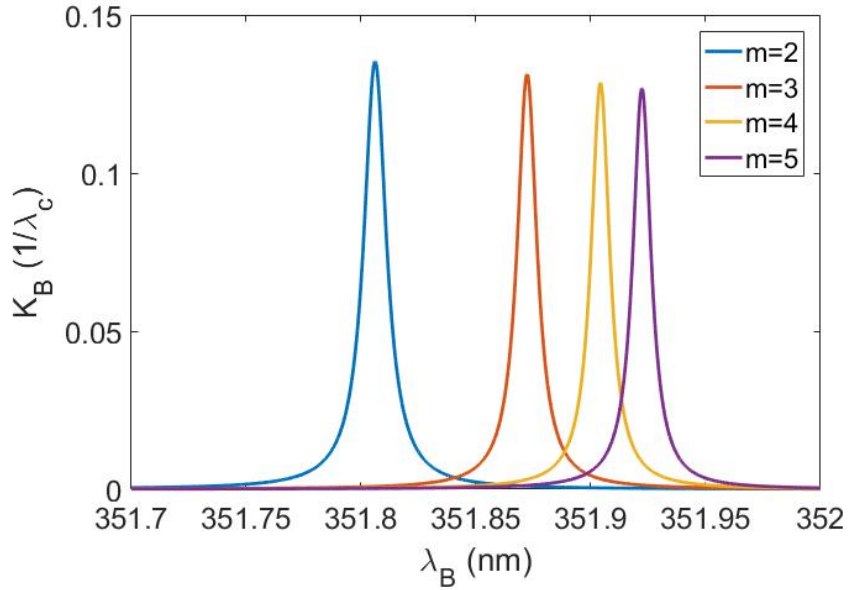


Figure 10: The convective spatial growth rate (κ_B) of SBS versus scattered wavelength (λ_B) at different super-Gaussian exponents m in fully ionized CO₂ plasma. The condition $n_e = 0.1 n_c$, $T_e = 3$ KeV, $T_i = T_e/5$ and $I_0 = 10^{15}$ W/cm² is taken.

Z [9]. For the typical condition $v_{th,i} \ll v_{ph} \ll v_{th,e}$, it can be expected the electron damping becomes more and more important compared to ion damping when increasing Z . In fact, it is found that for low- Z and intermediate- Z plasmas considered here, the ion damping dominates; while for high- Z plasma, the electron damping is more important. So in the following, we discuss the low- Z plasmas and high- Z plasmas, separately.

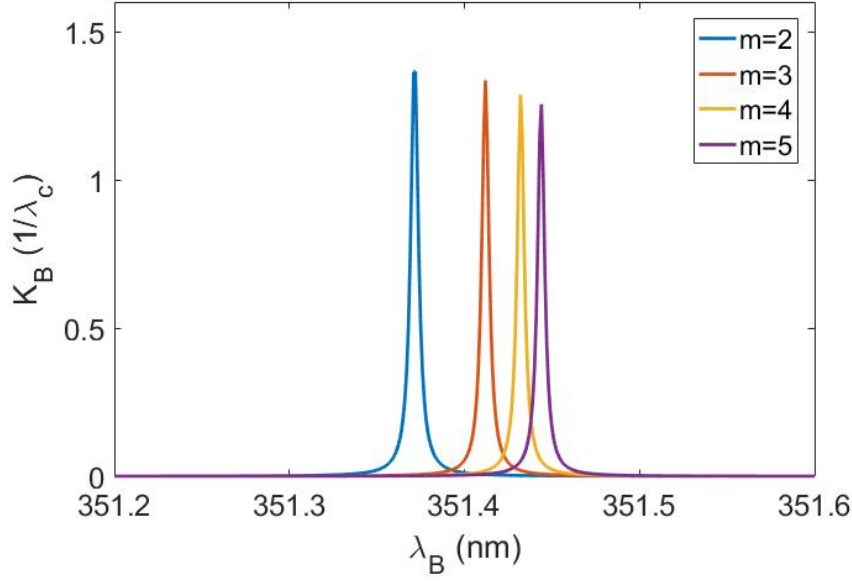


Figure 11: The convective spatial growth rate (κ_B) of SBS versus scattered wavelength (λ_B) at different super-Gaussian exponents m in Au plasma. The condition $n_e = 0.3 n_c$, $T_e = 1.5$ KeV, $T_i = T_e/5$, $Z_{Au} = 50$ and $I_0 = 10^{15}$ W/cm² is taken.

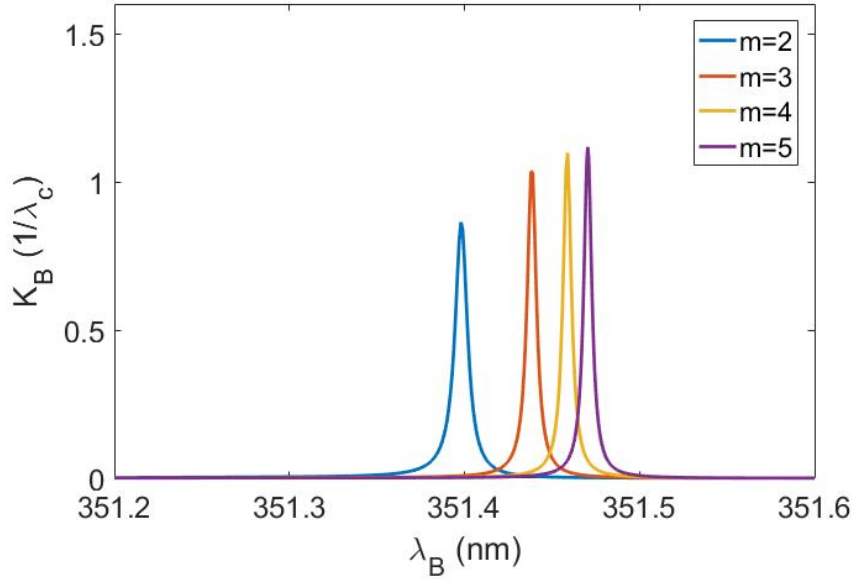


Figure 12: The convective spatial growth rate (κ_B) of SBS versus scattered wavelength (λ_B) at different super-Gaussian exponents m in AuB plasma. The condition $n_e = 0.3 n_c$, $T_e = 1.5$ KeV, Au/B=1:1, $T_i = T_e/5$, $Z_{Au} = 50$, $Z_B = 5$ and $I_0 = 10^{15}$ W/cm² is taken.

For low-Z plasmas, one noticeable feature is that even in both H and He plasma, the SBS gain increases with m , in H/He plasma, the SBS gain decreases with m . To understand this, we show \mathcal{D}^R and $-\mathcal{D}^I$ for He and H/He plasmas in Figure 14. It can be seen the influence of m on the damping versus λ_B can be ignored, since the damping is dominated by ion damping. Then, it is the dependence of the damping on λ_B near the best matching wavelength which determines

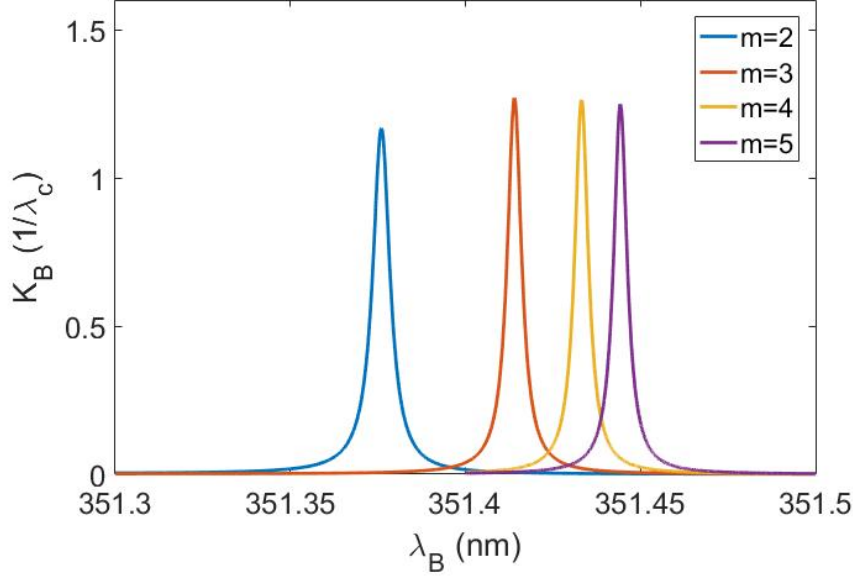


Figure 13: The convective spatial growth rate (κ_B) of SBS versus scattered wavelength (λ_B) at different super-Gaussian exponents m in UN plasma. The condition $n_e = 0.3 n_c$, $T_e = 1.5$ KeV, $U/N=1:1$, $T_i = T_e/5$, $Z_U = 50$, $Z_N = 7$ and $I_0 = 10^{15}$ W/cm² is taken.

the variation of the damping at the peak gain with m . For He plasma, the damping near the resonance decreases with λ_B , while for H/He plasma, it increases with λ_B . Consequently, in He plasma, the SBS peak gain increases with m , while in H/He plasma, the SBS peak gain decreases with m .

Similarly, we show \mathcal{D}^R and $-\mathcal{D}^I$ for high-Z Au and UN plasmas in Figure 15. In Au plasma, electron damping dominates. As in the SRS, the electron damping versus λ_B decreases with m . However, this dependence is weaker than the increase of the damping with λ_B . So in Au plasma, the increase of the best matching wavelength with m results in the decrease of the SBS gain with m . In UN plasma, the damping is contributed by both the electron damping, $\nu_e \propto -\mathcal{D}_e^I \equiv -\text{Im}[1/\chi_e]$, and the ion damping, $\nu_{\text{ion}} \propto -\mathcal{D}_{\text{ion}}^I \equiv -\text{Im}[1/(1 + \sum_{\alpha} \chi_i \alpha)]$. The former increases with λ_B , whereas the latter decreases with λ_B . The non-monotonic change of the gain with m is the combined effects of them.

In summary, the primary effect of a super-Gaussian EEDF on SBS is the reduce of low energy electrons to shield ions, which results in the increase of ion acoustic velocity and consequently, the increase of the frequency of IAW and the scattered wavelength of SBS. However, since the dependence of the damping of IAW on the frequency and wavenumber of IAW is quite complex, especially for multiple species plasmas, the SBS gain versus m demonstrates quite diverse behaviours according to the ion species and ion ratio.

4 Conclusion

By a linear analysis, we have found that the best matching wavelength and the spatial growth rate of both SRS and SBS processes are influenced by the Langdon effects which lead to a super-Gaussian EEDF. For SRS, a super-Gaussian EEDF changes the dispersion relation resulting in a redshift or blueshift of the best matching frequency depending on the plasma con-

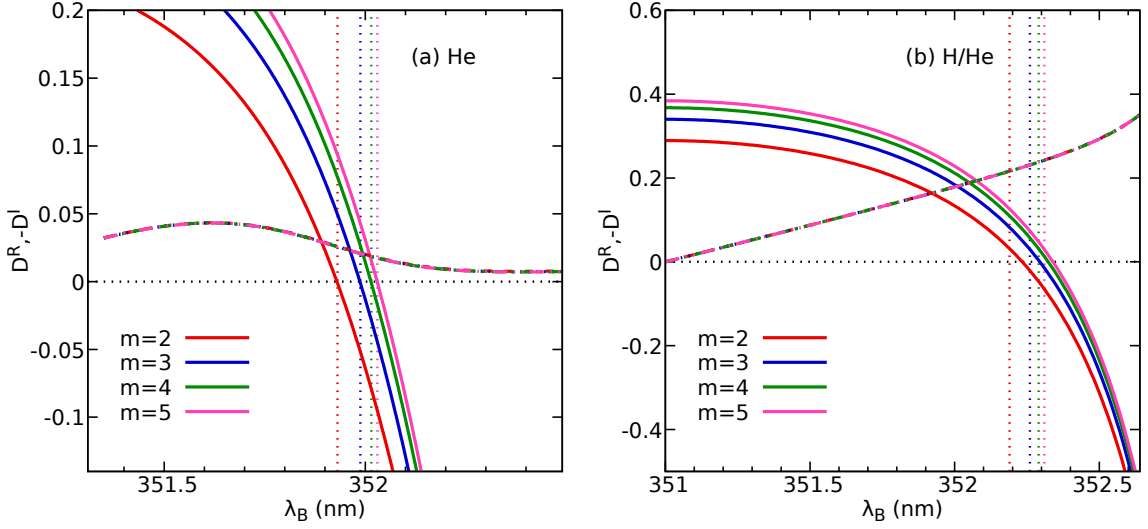


Figure 14: \mathcal{D}^R (solid line) and $-\mathcal{D}^I$ (dashed line) for (a) He plasma and (b) H/He plasma at different Gaussian exponents $m = 2$ (red curves), $m = 3$ (blue curves), $m = 4$ (green curves) and $m = 5$ (magenta curves). The locations of best matching wavelength of SBS for each m are indicated by the vertical dotted lines, at which $\mathcal{D}^R \approx 0$. (Notice that for H/He plasma, due to the large variation of \mathcal{D}^I with m near the best matching wavelength, there is a small deviation of \mathcal{D}^R from zero at the best matching wavelength.) $-\mathcal{D}^I$ is dominated by contributions from ions.

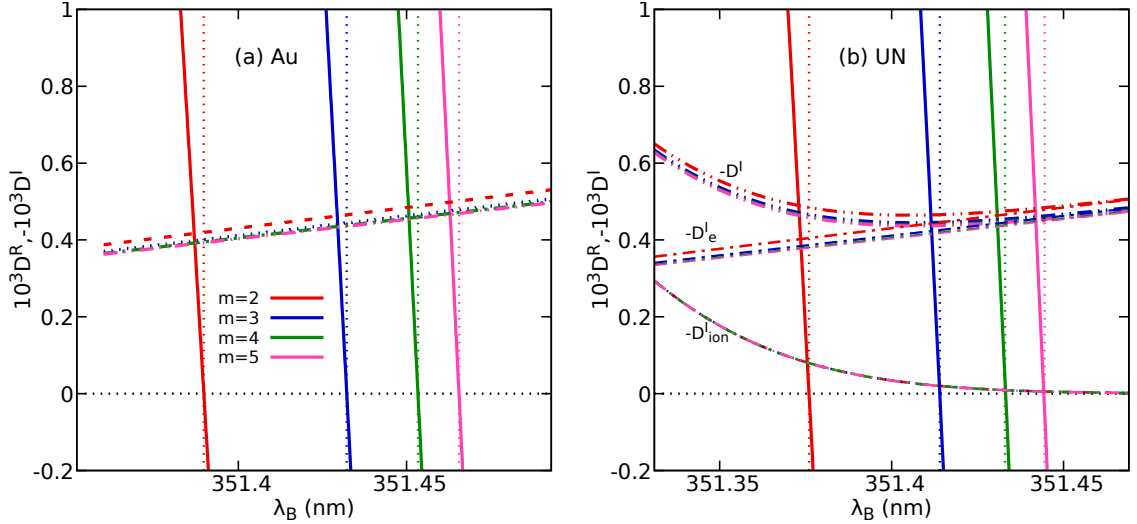


Figure 15: \mathcal{D}^R (solid line) and $-\mathcal{D}^I$ (dashed line) for (a) Au plasma and (b) UN plasma at Gaussian exponents $m = 2$ (red curves), $m = 3$ (blue curves), $m = 4$ (green curves) and $m = 5$ (magenta curves). The locations of best matching wavelength of SBS for each m are indicated by the vertical dotted lines, at which $\mathcal{D}^R \approx 0$. For Au plasma, $\mathcal{D}_{\text{ion}}^I \equiv \text{Im}[1/(1 + \sum_{\alpha} \chi_i \alpha)] \approx 0$, \mathcal{D}^I is nearly equal to $\mathcal{D}_e^I \equiv \text{Im}[1/\chi_e]$. For UN plasma, \mathcal{D}^I is contributed by both \mathcal{D}_e^I for electrons and $\mathcal{D}_{\text{ion}}^I$ for ions. So in (b), $-\mathcal{D}_e^I$ and $-\mathcal{D}_{\text{ion}}^I$ are also shown.

dition. On the other hand, a super-Gaussian EEDF always decreases the damping of EPW, thus increasing the gain of SRS. For SBS, a super-Gaussian EEDF takes effect mainly by reducing the low energy electron number to shield the ions, resulting in an effective increase of ion

acoustic frequency, and hence a redshift of SBS scattered wave. However, due to the complex behaviours of the IAW damping with respect to the ion acoustic frequency and wave number, the SBS gain shows quite diverse behaviours with the super-Gaussian exponent according to ion species, Z and ion ratio of the plasma.

References

- [1] John D. Lindl, Peter Amendt, Richard L. Berger, S. Gail Glendinning, Siegfried H. Glenzer, Steven W. Haan, Robert L. Kauffman, Otto L. Landen, and Laurence J. Suter. The physics basis for ignition using indirect-drive targets on the national ignition facility. Physics of Plasmas, 11(2):339–491, 2004.
- [2] Liang Hao, Yiqing Zhao, Dong Yang, Zhanjun Liu, Xiaoyan Hu, Chunyang Zheng, Shiyang Zou, Feng Wang, Xiaoshi Peng, Zhichao Li, Sanwei Li, Tao Xu, and Huiyue Wei. Analysis of stimulated raman backscatter and stimulated brillouin backscatter in experiments performed on sg-iii prototype facility with a spectral analysis code. Physics of Plasmas, 21(7):072705, 2014.
- [3] D. J. Strozzi, E. A. Williams, D. E. Hinkel, D. H. Froula, R. A. London, and D. A. Callahan. Ray-based calculations of backscatter in laser fusion targets. Physics of Plasmas, 15(10):102703, 2008.
- [4] A. Bruce Langdon. Nonlinear inverse bremsstrahlung and heated-electron distributions. Physical Review Letters, 44(9):575–579, 1980.
- [5] J P Matte, M Lamoureux, C Moller, R Y Yin, J Delettrez, J Virmont, and T W Johnston. Non-Maxwellian electron distributions and continuum X-ray emission in inverse Bremsstrahlung heated plasmas. Plasma Physics and Controlled Fusion, 30(12):1665–1689, 1988.
- [6] David Turnbull, Arnaud Colaitis, Aaron M. Hansen, Avram L. Milder, John P. Palastro, Joseph Katz, Christophe Dorrer, Brian E. Kruschwitz, David J. Strozzi, and Dustin H. Froula. Impact of the Langdon effect on crossed-beam energy transfer. Nature Physics, 16:181–185, 2020.
- [7] G. N. Hall, O. S. Jones, D. J. Strozzi, J. D. Moody, D. Turnbull, J. Ralph, P. A. Michel, M. Hohenberger, A. S. Moore, O. L. Landen, L. Divol, D. K. Bradley, D. E. Hinkel, A. J. Mackinnon, R. P. J. Town, N. B. Meezan, L. Berzak Hopkins, and N. Izumi. The relationship between gas fill density and hohlraum drive performance at the national ignition facility. Physics of Plasmas, 24(5):052706, 2017.
- [8] D. J. Strozzi, D. S. Bailey, P. Michel, L. Divol, S. M. Sepke, G. D. Kerbel, C. A. Thomas, J. E. Ralph, J. D. Moody, and M. B. Schneider. Interplay of laser-plasma interactions and inertial fusion hydrodynamics. Phys. Rev. Lett., 118:025002, 2017.
- [9] Francis F Chen. Introduction to plasma physics and controlled fusion, volume 1. Springer, 1984.
- [10] William L Kruer. The physics of laser plasma interaction, 1988.

- [11] J. F. Drake, P. K. Kaw, Y. C. Lee, G. Schmid, C. S. Liu, and Marshall N. Rosenbluth. Parametric instabilities of electromagnetic waves in plasmas. The Physics of Fluids, 17(4):778–785, 1974.
- [12] Bedros B. Afeyan, Albert E. Chou, J. P. Matte, R. P. J. Town, and William J. Kruer. Kinetic theory of electron-plasma and ion-acoustic waves in nonuniformly heated laser plasmas. Phys. Rev. Lett., 80:2322–2325, 1998.